JOURNAL OF MAGNETIC RESONANCE **131,** 286–294 (1998)
ARTICLE NO. MN981369

Multilayer Gradient Coil Design

R. Bowtell and P. Robyr[1]

Magnetic Resonance Centre, Department of Physics, University of Nottingham, University Park, Nottingham NG7 2RD, United Kingdom

Received July 28, 1997; revised December 22, 1997

In standard cylindrical gradient coils consisting of wires wound in a single layer, the rapid increase in coil resistance with efficiency is the limiting factor in achieving very large magnetic field gradients. This behavior results from the decrease in the maximum usable wire diameter as the number of turns is increased. By adopting a multilayer design in which the coil wires are allowed to spread out into multiple layers wound at increasing radii, a more favorable scaling of resistance with efficiency is achieved, thus allowing the design of more powerful gradient coils with acceptable resistance values. By extending the theory used to design standard cylindrical gradient coils, we have developed mathematical expressions which allow the design of multilayer coils, and the evaluation of their performance. These expressions have been used to design a four-layer, *z*-gradient coil of 8 mm inner diameter, which has an efficiency of 1.73 Tm^{-1} A^{-1}, a resistance of 1.8 Ω, and an inductance of 50 μH. This coil produces a gradient which deviates from linearity by less than 5% within a central cylindrical region of 4.5 mm length and 4.5 mm diameter. A coil has been constructed from this design and tested in simple imaging and pulsed gradient spin echo experiments. The resulting data verify the predicted coil performance, thus demonstrating the advantages of using multilayer coils for experiments requiring very large magnetic field gradients.

Key Words: **NMR; gradient coil; PGSE; microscopy.**

INTRODUCTION

Very large magnetic field gradients are required in a variety of NMR experiments. NMR microscopy and pulsed gradient spin echo (PGSE) experiments can particularly benefit from the availability of switchable gradients of more than 10 Tm^{-1} strength. In NMR microscopy large field gradients are needed to achieve fine resolution, particularly in the ''diffusion-limited'' regime, where diffusion under the read gradient is the dominant broadening mechanism (*1*). In PGSE experiments, strong gradients in the field are necessary for the measurement of diffusion in low-mobility systems and also allow the investigation of motion occurring on short timescales (*2*).

Very large magnetic field gradients for use in NMR experiments can be generated by specially designed superconducting magnets (*3*), but also occur naturally in the fringe fields of conventional high field superconducting magnets. Chang *et al.* used an ''anti-Helmholz'' arrangement of superconducting coils, which gives a gradient of approximately 180 Tm^{-1}, in a variety of experiments carried out on systems with low mobility (*3*). The maximum rate of change of field with position below a 400-MHz, 89-mm bore superconducting magnet is about 60 Tm^{-1} (*4*). Such gradients in the stray field have been widely employed in STRAFI (*4*) experiments and in diffusion measurements (*5*). Use of these systems in gradient generation has the advantage of giving large, highly stable gradients over reasonably large volumes, but the disadvantage of only providing a fixed magnitude gradient which cannot be switched off. The permanent presence of the gradient poses severe lower limits on the bandwidth of the RF pulses which must be used in NMR experiments and also restricts the range of pulse sequences which can be implemented. Magnetic field gradients of similar magnitude, which can be rapidly switched on and off, and varied in magnitude offer some considerable advantages.

To date, most experiments employing very large, switched magnetic field gradients have been based on the use of quadrupolar gradient coils (*6–8*). Three recent designs give gradient strengths of 1.05 Tm^{-1} A^{-1} for samples with a maximum diameter of 1.5 mm (*6*), 0.21 Tm^{-1} A^{-1} for samples of 2.7 mm maximum diameter (*7*), and 0.28 Tm^{-1} A^{-1} with samples in standard 5-mm NMR tubes (*8*). Quadrupole gradient coils are based on wires wound around the surface of a cylinder, whose axis is normal to the applied magnetic field. This type of coil generates a gradient in a direction normal to the axis of the coil. The quadrupole coil geometry has certain disadvantages for sample mounting, since in vertical bore magnets the sample must be mounted horizontally. Orientation of the sample with respect to the gradient direction is also not as straightforward as it is when using a conventional gradient coil, in which the coil cylinder axis is parallel to the applied field.

In this paper we describe a new method of building very strong magnetic field gradient coils with low resistance and consequent power dissipation, which have standard geometry. Although this method is potentially applicable to the

[1] Current address: Laboratorium für Physikalische Chemie, Universitaetsstrasse 22, ETH-Zentrum, CH-8092 Zürich, Switzerland.

1090-7807/98 $25.00

design of coils which will generate gradients in the z component of the magnetic field along any of the three Cartesian axes, here we describe the application to z gradient coils only.

THEORY

In designing a gradient coil there is always a tradeoff between the gradient strength per unit current (usually known as the gradient coil efficiency), η, inductance, L, resistance, R, and the size of the region within which the field variation is linear with position. Increased efficiency usually leads to worse linearity, higher inductance which in turn implies longer gradient rise-times, and higher resistance, resulting in greater power dissipation in the coil (9). As is shown below, the scaling of the above parameters with coil size means that the highest coil performance can be achieved using small coils and that for such coils the resistance, and consequent power dissipation in the coil, constitute the limiting factor in achieving high gradient strengths.

In constructing a gradient coil, the required current paths may be formed from wires or by making cuts in a conductive layer. With small cylindrical coils (<2 cm in radius) the latter approach is technically difficult, because of problems of machining at such small scale, and also because the removal of conducting material by cutting inevitably leads to low current-carrying cross sections in regions of the coil where a high current density is required. For small, highly efficient coils, wire winding is thus the usual method of construction.

For a cylindrical coil of radius a, consisting of n turns of wire of diameter d, wound in a single layer, the following scaling relationships hold

$$\eta \propto \frac{n}{a^2},\ L \propto n^2 a,\ R \propto \frac{na}{d^2}. \qquad [1]$$

These mean that for a given peak gradient strength and rise-time, the required amplifier power, $V_a I_a$, and the power dissipated in the coil, P, show the following behavior:

$$V_a I_a \propto \frac{L}{\eta^2} \propto a^5,\ P \propto \frac{R}{\eta^2} \propto \frac{a^5}{nd^2}. \qquad [2]$$

The considerable gains in performance which result upon reducing the coil radius, a, are obvious from the above equations. Unfortunately the reduction in resistance and power dissipation for very small coils is not as dramatic as might be simply deduced from the form of Eqs. [1] and [2]. This is a consequence of the reduction in the minimum usable wire diameter as the coil size is reduced. Generally the largest wire diameter which can be used is set by the minimum wire spacing in the coil pattern. For a given coil design, which is defined by the current distribution that the wire paths are designed to mimic, this spacing is proportional to the coil radius and inversely proportional to n.

Equations [1] and [2] make it clear that in order to maximize the gradient strength produced by a gradient coil, it is sensible to construct the smallest coil which will accommodate the RF coil and sample, to use the maximum amplifier current I_a, and to maximize the number of turns, n, on the coil. There are however two main constraints, besides that of the feasibility of coil construction, which limit the maximum attainable value of n.

Inductance. For large gradient coils, the rapid increase in inductance with n is usually the limiting factor. As n is increased the inductance eventually becomes so large that it is not possible to achieve an acceptable gradient rise time

$$\tau \approx \frac{LI_a}{V_a}. \qquad [3]$$

Resistance. For smaller coils in which the size dependence naturally yields a low inductance, the coil resistance is the limiting factor. As n is increased, the coil resistance rises and the voltage needed to pass the maximum current through the coil increases until

$$R = \frac{V_a}{I_a}. \qquad [4]$$

For larger values of n, there is no further gain in gradient strength because the maximum current is limited by the resistance and maximum output voltage.

In a coil where the wire diameter is limited by the minimum wire spacing, the resistance increases rapidly with n

$$R \propto \frac{n^3}{a}, \qquad [5]$$

so that for a fixed coil radius

$$\eta \propto R^{1/3}. \qquad [6]$$

This means that doubling the efficiency of the coil by using twice as many turns results in an eightfold increase in the resistance (a factor of two due to the increased wire length and a factor of four due to the reduction in current-carrying cross sections, as shown in Fig. 1a). The rapid scaling of resistance with the number of turns poses a severe limit on the attainable gradient strength. It results mainly from the unnecessarily rapid reduction in current-carrying cross sections with increasing n. This problem can be overcome by adopting a multilayer coil design in which the wires are allowed to spread out in the radial direction. In this situation,

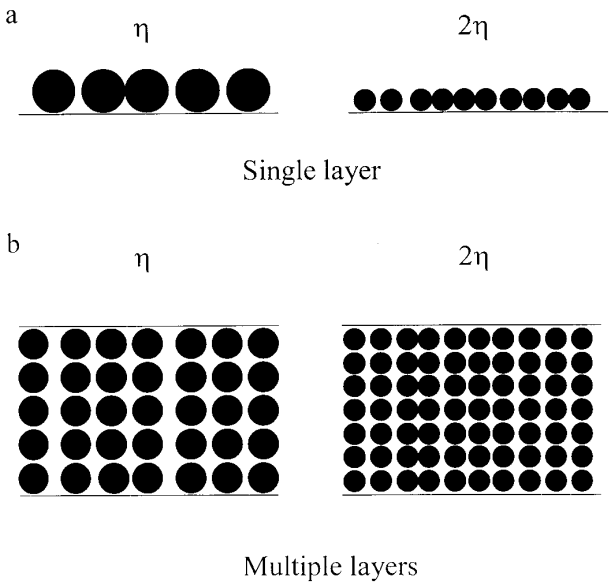

FIG. 1. To double the efficiency of a coil of fixed radius it is necessary to double the number of turns. (a) In a single-layer coil this leads to a factor of four reduction in the current-carrying cross section. (b) In a multilayer coil the doubling can be achieved by a $\sqrt{2}$ reduction in the wire diameter and a $\sqrt{2}$ increase in the number of layers.

with the inner and outer radii of the layers fixed, the efficiency scales as

$$\eta \propto R^{1/2}, \quad [7]$$

so that as illustrated in Fig. 1B, doubling the efficiency via a factor of two increase in n causes only a fourfold increase in R (a factor of two due to the increased wire length and a factor of two due to the $\sqrt{2}$ reduction in wire diameter). This behavior opens up access to much higher gradient strengths at reasonable coil resistance and power dissipation.

The design of multilayer gradient coils requires minor extension to the theory used to design standard single-layer cylindrical coils (*9*). A multilayer cylindrical coil confined between radii ρ_i and ρ_0 ($\rho_i < \rho_0$) can be described by a current distribution $\underline{j}(\phi, \rho, z)$, which is zero for $\rho > \rho_0$ and $\rho < \rho_i$. The analysis presented here is limited to current distributions which have only azimuthal and axial components, since the presence of a radial component will make coil construction difficult. Further work on exploring the feasibility of using all three components of the current distribution is currently in progress. For such a current distribution, the magnetic field in the region $\rho < \rho_i$ is given by

$$B_z(\rho, \phi, z) = -\frac{\mu_0}{2\pi}\int_{\rho_i}^{\rho_0} d\rho' \rho' \sum_{m=-\infty}^{\infty}\int_{-\infty}^{\infty} kdk\, j_\phi^m(\rho', k) \times e^{ikz}e^{im\phi}K_m'(k\rho')I_m(k\rho), \quad [8]$$

where $j_\phi^m(\rho, k)$ is the Fourier transform of the azimuthal component of $\underline{j}$, with respect to ϕ and z,

$$j_m^\phi(\rho, k) = \frac{1}{2\pi}\int_{-\infty}^{\infty} dz \int_0^{2\pi} d\phi j_\phi(\rho, \phi, z)e^{-im\phi}e^{-ikz}, \quad [9]$$

while I_m and K_m are the modified Bessel functions. The power dissipated by this current distribution is

$$P = \int_{\rho_i}^{\rho_0} \rho d\rho \sum_{m=-\infty}^{\infty}\int_{-\infty}^{\infty} dk \frac{1}{\sigma} |j_\phi^m(\rho, k)|^2 \times \left(1 + \frac{m^2}{k^2\rho^2}\right), \quad [10]$$

where σ is the electrical conductivity of the medium in which the current flows. The inductance is given by the more complicated expression

$$L = -\frac{\mu_0}{I^2}\int_{\rho_i}^{\rho_0} \rho d\rho \sum_{m=-\infty}^{\infty}\int_{-\infty}^{\infty} dk (j_\phi^m(\rho, k))^*(I_m'(k\rho) \times \int_{\rho}^{\rho_0} d\rho' \rho' K_m'(k\rho') j_\phi^m(\rho', k) + K_m'(k\rho)\int_{\rho_i}^{\rho} d\rho' \rho' I_m'(k\rho') j_\phi^m(\rho', k)), \quad [11]$$

where the first term in the parentheses corresponds to the mutual inductance between a given layer and all layers found at greater radii, while the second term corresponds to the mutual inductance with the layers at lesser radii. I is the current passed by the coil. These equations are applicable to transverse and longitudinal gradient coils, with the former being based solely on terms $j_\phi^m(\rho, k)$ with $m = \pm 1$, while the latter require only the $m = 0$ term, as is the case with standard cylindrical coils. If active screening (*10*) is to be incorporated, so that the field at radii $\rho > \rho_0$ is zero, the current distribution must fulfill the equation

$$\int_{\rho_i}^{\rho_0} d\rho \rho I_m'(k\rho) j_\phi^m(\rho, k) = 0. \quad [12]$$

METHOD

Using the theory described above, it is possible to implement the full range of analytical methods for the design of gradient coils (*9*), including the target field (*11*), minimum inductance (*12*), and minimum power (*13*) approaches. For designing a strong, longitudinal unscreened gradient coil, we have adopted a different approach in which a weighted combination of the inductance, power dissipation, and gradient homogeneity is optimized. This approach is similar to that employed by Carlson (*14*) in the design of standard

cylindrical coils. To design a coil of length, $2l$, the current distribution, $\underline{j}$, is initially divided into a number of equally spaced layers, N. In each layer the current distribution is generated from Q axial harmonics. In the case of a z gradient coil $\underline{j}$ has only an azimuthal component which is given by

$$j_\phi(\rho, z) = \sum_{n=1}^{N} \delta(\rho - \rho_n) \sum_{q=1}^{Q} \lambda_{nq} \sin\left(\frac{q\pi z}{l}\right) \quad [13]$$

in the region $-l < z < l$ and is zero elsewhere. After Fourier transformation this gives

$$j^0_\phi(\rho, k) = \sum_{n=1}^{N} \delta(\rho - \rho_n) \sum_{q=1}^{Q} \lambda_{nq} g_q(k), \quad [14]$$

where

$$g_q(k) = i(\mathrm{sinc}(kl + \pi q) - \mathrm{sinc}(kl - \pi q)). \quad [15]$$

We can define the internal field generated per unit amplitude by the qth harmonic in the nth layer as

$$b_{nq}(\rho, z) = -\frac{i\mu_0}{\pi} \int_0^\infty dk \rho_n k \sin(kz) K_1(k\rho_n) I_0(k\rho) g_q(k). \quad [16]$$

To design a coil, a region of homogeneity is first specified in the form of a grid of P points (ρ_p, z_p) at which the gradient linearity will be monitored. An optimal coil can then be generated using the above equations by calculating the coefficients, λ_{nq}, which minimize a weighted combination, Γ, of P, L, and the sum of the squares of the deviation of the field from a perfect gradient over the grid of points:

$$\Gamma = \alpha P + \beta L + \sum_{p=1}^{P} (Gz_p - B_z(\rho_p, z_p))^2. \quad [17]$$

Here α and β are constants whose values set the relative importance of the power dissipation and inductance in the minimization process.

The values of λ_{nq} which minimize Γ are found by solving the set of $n \times q$ first-order simultaneous equations produced by forcing all $\partial\Gamma/\partial\lambda_{nq}$ to zero. These can be written in matrix form as

$$\mathbf{B}\underline{\lambda} = \mathbf{A} \quad [18]$$

For simplicity we denote the matrix element coefficients as (nq), where n is the layer number and q is the harmonic number. It can be shown that $B_{(nq)(n'q')}$ and $A_{(nq)}$ are then given by

$$A_{(nq)} = \sum_{p=1}^{P} Gz_p b_{nq}(\rho_p, z_p) \quad [19]$$

and

$$B_{(nq),(n'q')} = \sum_{p=1}^{P} b_{nq}(\rho_p, z_p) b_{n'q'}(\rho_p, z_p) + \frac{4\alpha}{\sigma t} \rho_n \delta_{n,n'} \int_0^\infty dk g^*_q(k) g_{q'}(k) - 4\beta\mu_0 \rho_n \rho_{n'} \int_0^\infty dk g^*_q(k) g_{q'}(k) I_1(k\rho_<) K_1(k\rho_>), \quad [20]$$

where t is the thickness of each layer, $\delta_{n,n'}$ is the Kronecker delta, while $\rho_>$ and $\rho_<$ correspond to the larger and smaller of the two radii, ρ_n and $\rho_{n'}$.

The merit of the resulting current distribution can be assessed by calculating the values of η^2/L and η^2/R $(=G^2/P)$, as well as the field variation within the desired region of homogeneity, using Eqs. [8], [10], and [11]. The wire positions for the actual coil design are calculated by finding equally spaced contours of the stream function, S (*9*), in each layer. In a z gradient coil, the stream function is simply given by the integral of j_ϕ with respect to z. The procedure described above gives rise to a coil in which the turns in all layers can be simply connected in series. However, since the total integrated current in one-half of each individual layer is not necessarily related to that in any other layer by a ratio of integers, the current distributions need to be slightly modified so that an integral number of turns in each layer will correctly represent the required current distribution. This modification can be accomplished by introducing positive and negative delta function singularities of appropriate magnitude at the zero crossing of j_ϕ at $z = 0$ (*14*), in all layers bar one (usually the innermost layer). In fact for the large numbers of turns used in our actual design this procedure was unnecessary, because imperfect representation of the total integrated current caused <1% perturbation of the field within the coil's homogeneous volume. The field variation due to the final coil design can be calculated using the Biot–Savart equation in the standard manner (*9*).

RESULTS

The main aim of this work was the production of a very strong, z gradient coil, which would accommodate samples contained in standard 5-mm NMR tubes, operate in a static magnetic field of 11.7 T, and interface to an existing NMR microscope (*15*). The latter uses two parallel M600 amplifiers (Crown International) to drive each gradient coil. These

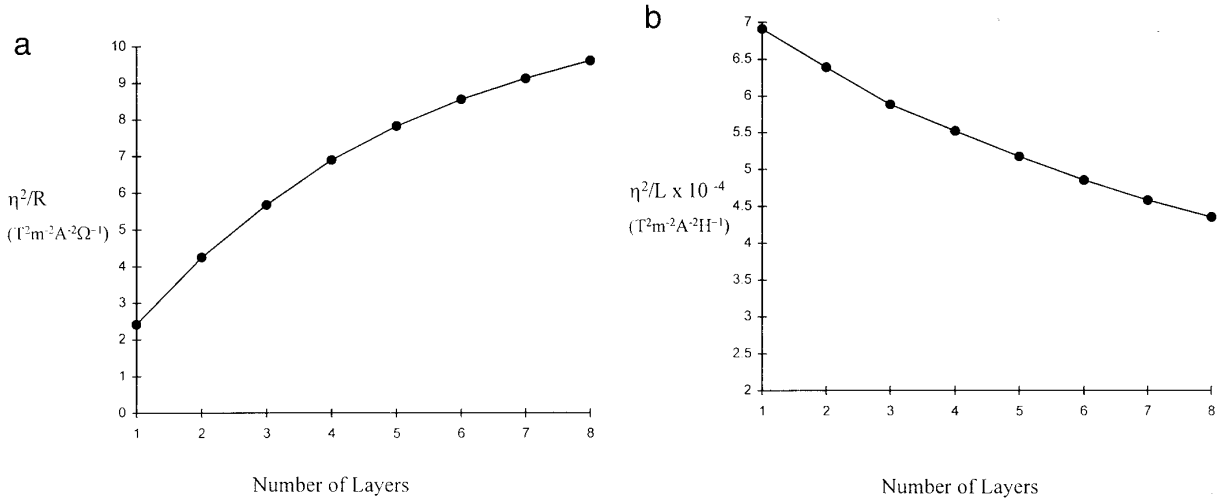

FIG. 2. The variation of (a) η^2/L and (b) η^2/R, with the number of layers in the current distribution. The coil design parameters are given in the text.

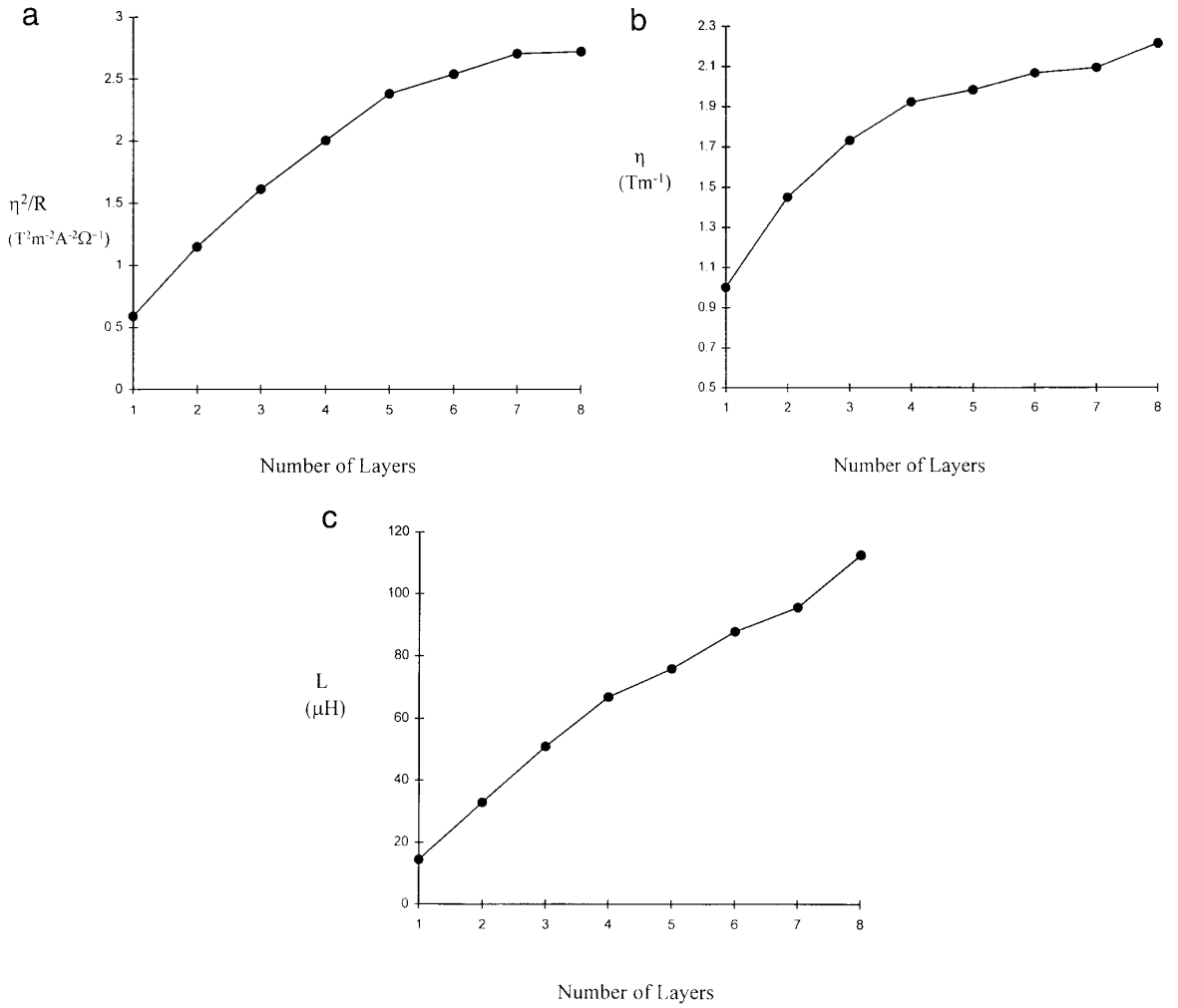

FIG. 3. The variation of (a) η^2/R, (b) η, and (c) L, with the number of layers in the coil design composed of discrete wires. The design parameters are given in the text.

TABLE 1
Data from Coils with a Varying Number of Layers

No. of layers	No. of turns per layer	η (Tm^{-1} A^{-1})	R (Ω)	η^2/R (T^2 m^{-2} A^{-2} Ω^{-1}	L (μH)
1	32	1.00	1.70	0.59	14
2	26, 23	1.45	1.83	1.15	33
3	23, 20, 17	1.73	1.85	1.61	51
4	21, 18, 16, 14	1.92	1.84	2.00	67
5	19, 16, 14, 13, 11	1.98	1.65	2.39	76
6	18, 16, 14, 12, 11, 9	2.06	1.68	2.53	88
7	17, 15, 13, 11, 10, 9, 3	2.09	1.62	2.70	95
8	17, 15, 13, 11, 10, 9, 8, 7	2.21	1.80	2.713	112

Note. The design parameters are given in the text.

are capable of providing a peak output of 50 amp at 100 V. We consequently aimed for a gradient coil with an inner diameter of 8 mm, which provided a usable volume within which the gradient deviated from linearity by less than 5%, consisting of a 4.5-mm diameter cylinder of 4.5 mm length, and which had a resistance of approximately 2 Ω and an inductance of less than 100 μH. The coil length and outer diameter were not significantly constrained. In the light of above we initially opted for an inner layer centered at a radius of 4.5 mm and a layer thickness of 0.36 mm. This gives a unity ratio of the length and diameter of the cylindrical region of homogeneity to the inner layer radius.

Figure 2 shows the variation of η^2/R and η^2/L with the number of layers in the coil. These values are calculated directly from the current distribution, assuming $\sigma = 1.71 \times 10^{-8}$ Ωm. In each case the current distribution was calculated as that which gave the minimum value of R/η^2 while just fulfilling the homogeneity requirements. This was accomplished by varying α, with β set equal to 0. The absolute values of η^2/L calculated in this manner are expected to be very similar to those given by a wire wound coil. As indicated by Fig. 3, η^2/R values for wire wound coils are significantly lower than those calculated using the continuous current distribution, because of the reduced effective current-carrying cross section which inevitably results from the use of wires. The trend of increasing efficiency with the number of layers at fixed resistance is, however, clear from both figures. Figure 2b indicates that the inductance at fixed efficiency increases as the number of layers goes up for this type of unscreened coil. This agrees with earlier work (*16*) which indicates that a single-layer unscreened coil generally has an inductance lower than that of a multilayer coil.

Wire positions were calculated from these current distributions, with the number of wires chosen to give a resistance falling between 1.6 and 1.9 Ω. Figure 3 shows the values of η^2/R, η, and L calculated for the resulting coils. In calculating the resistance of each coil it was assumed that the wire diameter was the same in all layers and equal to the minimum spacing of wires in the inner layer. The latter assumption will lead to an underestimation of the resistance of a real coil because of the necessary inclusion of a layer of insulation on the wires. Values of η were calculated using the Biot–Savart equation. Inductances were derived from the efficiency values and those of η^2/L. The numerical values are shown in Table 1.

Figure 3b shows the considerable increase in η which can be achieved by increasing the number of layers. The rapid growth in L with n shown in Fig. 3c results both from the reduction in η^2/L and the increased magnitude of η. Figure 3b indicates a reduction by a factor of between 3.5 and 4 in η^2/R for the wire wound coil, compared with the continuous current distribution. It should however be borne in mind that a coil constructed by cutting conducting layers would also suffer a significant reduction in η^2/R because of removal of the conducting layer. In the single-layer coil, for example, it would be necessary to generate a cut thickness of less than 60 μm in order to achieve a similar resistance to the wire wound coil.

After consideration of the data shown in Fig. 3 we chose to build a four-layer coil design, as a compromise between ease of construction and maximum achievable gradient strength. To produce a coil which was feasible to construct, it was necessary to slightly reduce the number of turns in each layer compared with those given in Table 1, and to use a somewhat smaller wire diameter than that set by the minimum spacing of turns. The final coil design has a total of 120 turns made of 0.224-mm diameter copper wire. The wire positions are shown in Fig. 4. The calculated efficiency, resistance, and inductance of this coil design are 1.8 Ω, 49 μH, and 1.65 Tm^{-1} A^{-1}, respectively. The spatial variation of the field generated by the coil is displayed in Fig. 5, which shows contours of $(B_z/Gz - 1)$ at multiples of 5%. The central homogeneous volume within which the field deviates from linearity by less than 5% can be clearly seen.

The coil was wound on a glass-reinforced plastic former with an 8-mm diameter bore. At the start of the process of

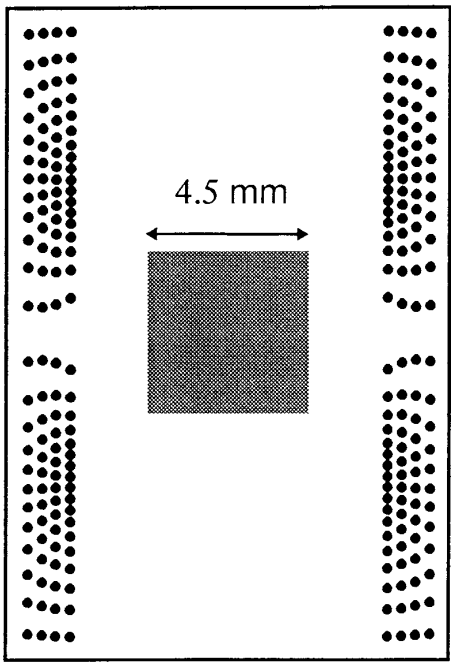

FIG. 4. The wire positions in the 120-turn coil design are indicated on this longitudinal cross section through the coil.

coil construction, the central region of the former was turned down to an outer diameter of 9 mm, and grooves defining the wire paths were cut into the former surface. The wire was then wound into these grooves and periodically fixed in place with cyanoacrylate glue. The pitch and depth of the cuts ensured that the wire centers were located at a diameter of 9 mm. Once one layer had been wound, the former was

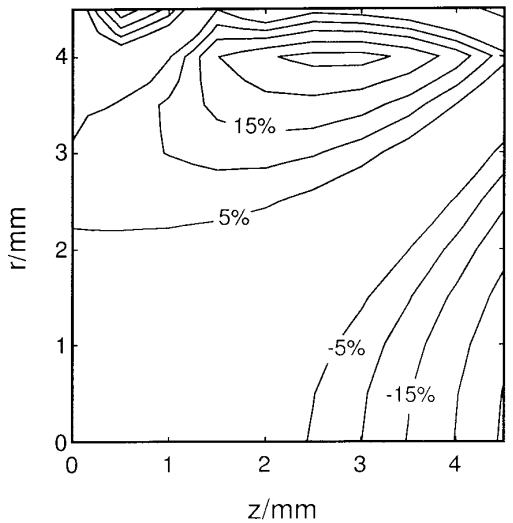

FIG. 5. The variation of $(B_z/Gz - 1)$ for the coil of Fig. 4 is shown in this contour plot. Contour levels are set at 5% intervals. The field variation was calculated from the wire positions using the Biot–Savart equation.

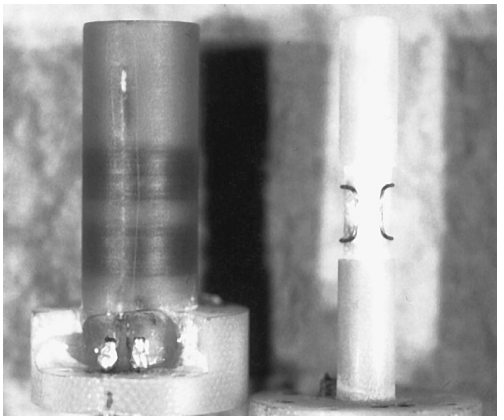

FIG. 6. A picture of the completed coil assembly showing the gradient coil (left) and the RF coil insert (right).

immersed in epoxy resin, and held under vacuum and at 60°C for 24 h while the resin set. The resin was then turned down to a diameter of 9.72 mm, and the grooves for the next layer were cut. The wires in the second layer were wound in the opposite direction to those in the first, so that simply connecting together the turns most offset from the coil center in both layers gave the same sense of current flow in both layers. After covering the coil in epoxy once more, the whole process was repeated for the third and fourth layers. The outer diameter of the finished coil was 15 mm. A short, saddle RF coil with a sensitive volume matched to the homogeneous region of the gradient coil was wound on a former with 6 mm outer diameter and 5 mm inner diameter. Figure 6 shows a picture of the completed coil assembly.

Using an LCR meter, the coil was determined to have an inductance of 49.4 ± 0.5 μH and a resistance of 1.76 ± 0.01 Ω. Both numbers are in good agreement with the calculated values. The coil efficiency was measured using a simple one-dimensional imaging experiment. Figure 7a shows a one-dimensional profile of a phantom whose form is shown in Fig. 7b. The 512-point profile was acquired using a simple spin-echo sequence with an acquisition window of 2.048 ms duration and a current of 0.58 amp passing through the coil. Using the known 400-μm separation of the groove centers, the coil efficiency is calculated to be 1.73 ± 0.05 $\mathrm{Tm^{-1}\,A^{-1}}$. This is approximately 5% larger than the theoretical value, but such a discrepancy could be explained by an error of less than 2% in the layer radii.

As a test of the coil's performance in generating large field gradients, we measured the diffusion coefficient of glycerol at room temperature. A simple spin-echo sequence incorporating two gradient pulses of 314 μs duration separated by 32.4 ms was employed. Figure 8 shows the measured variation of echo amplitude with coil current squared. The resulting diffusion coefficient was calculated as $1.02 \times 10^{-12} \pm 0.03\ \mathrm{m^2\,s^{-1}}$ which is in agreement with previously published values (*17*).

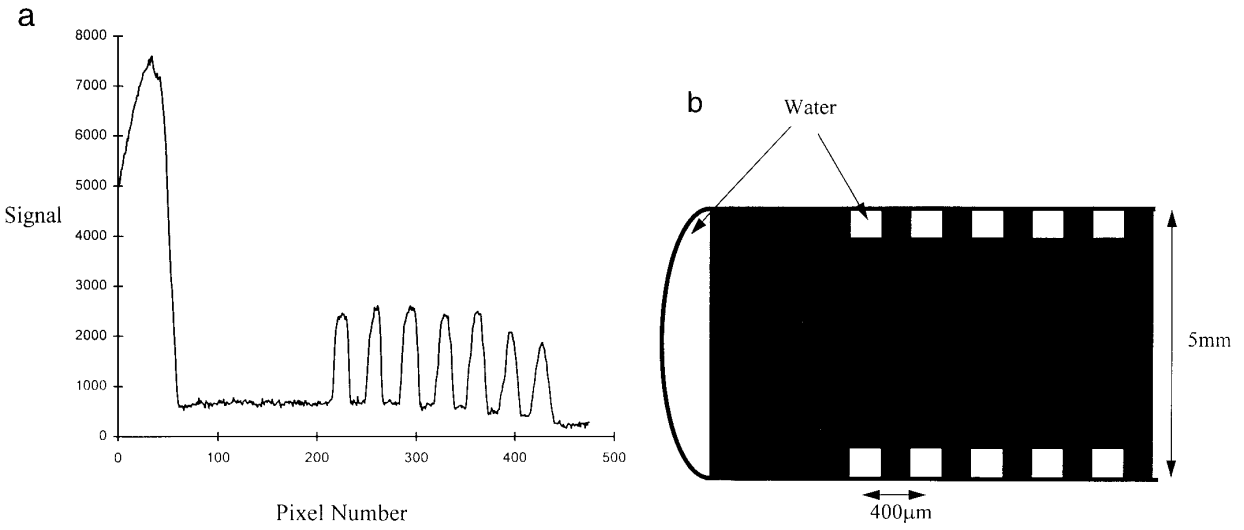

FIG. 7. (a) One-dimensional profile of a simple phantom taken in the *z* direction using a spin-echo sequence. The 512-point profile has a resolution of 11.4 μm. (b) The phantom consists of an epoxy resin plug of 4.1 mm outer diameter which was inserted into a water-filled, 5-mm NMR tube. The resin carries six water-filled grooves of 200 μm width and 500 μm depth whose centers are separated by 400 μm. There is also a 1-mm thick groove which runs along the length of the resin insert. Water in this groove gives rise to the small baseline level seen in the profile.

CONCLUSIONS

We have developed a framework for designing multilayer cylindrical gradient coils. This allows the generation of coils which have an efficiency at fixed resistance significantly higher than that of standard single-layer coils. This approach has been used to design a *z* gradient coil unit which accepts samples contained in 5-mm NMR tubes. The coil has four layers which give an efficiency of 1.73 $Tm^{-1} A^{-1}$, an inductance of 50 μH, and a resistance of about 1.8 Ω, with a cylindrical homogeneous volume within, which the field deviates from linearity by less than 5%, of 4.5 mm length and 4.5 mm diameter. A single-layer coil with a similar efficiency and homogeneous volume would have a resistance of over 8 Ω. The four-layer coil has been constructed and its performance tested via simple one-dimensional imaging experiments and the measurement of the diffusion coefficient of glycerol (*18*). This coil is now being used to measure spatially resolved diffusion coefficients in very low-mobility systems (*19*). The maximum current which has so far been used with this coil is 30 amp, giving a gradient of 52 Tm^{-1}.

The multilayer approach to coil design should also be applicable to transverse gradient coils, leading to similar gains in coil performance. Such coils are however likely to be harder to construct because the links between layers will need to be made at a less favorable position (the centers of the individual fingerprint units) if space is not to be wasted by the inclusion of linking wires.

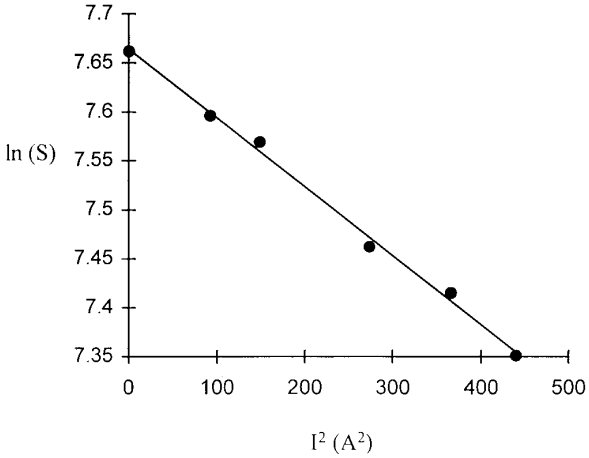

FIG. 8. The variation of signal amplitude with the square of gradient coil current in a PGSE experiment carried out on glycerol at room temperature. The experiment used two gradient lobes of 314 μs duration and 30.48 ms separation.

ACKNOWLEDGMENT

This work is supported by EPSRC Grant GR/H 96980.

REFERENCES

1. P. T. Callaghan, Diffusion limited resolution in NMR microscopy, *J. Magn. Reson.* **78,** 1–8 (1988).
2. P. P. Mitra, P. N. Sen, and L. M. Schwartz, Time-dependent diffusion-coefficient of fluids in porous-media as a probe of surface to volume ratio, *Phys. Rev. B* **47,** 8565–8574 (1993).
3. I. Chang, F. Fujara, B. Geil, G. Hinze, H. Sillescu, and A. Tölle, New perspectives of NMR in ultrahigh static magnetic field gradients, *J. Non-Cryst. Solids* **172–174,** 674–681 (1994).

4. P. J. McDonald, Stray field magnetic resonance imaging, *Prog. NMR Spectrosc.* **30,** 69–99 (1997).
5. R. Kimmich, W. Unrath, G. Schnur, and E. Rommel, NMR measurement of small self-diffusion coefficients in the fringe field of superconducting magnets, *J. Magn. Reson.* **91,** 136–140 (1991).
6. J. S. Schoeniger and S. J. Blackband, The design and construction of a NMR microscopy probe, *J. Magn. Reson. B* **104,** 127–134 (1994).
7. C. J. Rofe, J. Van Noort, P. J. Back, and P. T. Callaghan, NMR microscopy using large, pulsed magnetic-field gradients, *J. Magn. Reson. B* **108,** 125–136 (1995).
8. O. Oishi and S. Miyajima, New PFG NMR spectrometer with a rotatable quadrupole coil for the measurement of an anisotropic self-diffusion coefficient tensor, *J. Magn. Reson. A* **123,** 64–71 (1996).
9. R. Turner, Gradient coil design: A review of methods, *Magn. Reson. Imaging* **11,** 903–920 (1993).
10. P. Mansfield and B. Chapman, Active magnetic screening of gradient coils in NMR imaging, *J. Phys. E* **15,** 235–239 (1986).
11. R. Turner, A target field approach to optimal coil design, *J. Phys. D* **19,** L147–L151 (1986).
12. R. Turner, Minimum inductance coils, *J. Phys. E* **21,** 948–952 (1988).
13. R. Bowtell and P. Mansfield, Abstracts of the Society of Magnetic Resonance in Medicine, 8th Annual Meeting, Amsterdam, p. 977, 1989.
14. J. W. Carlson, K. A. Derby, K. C. Hawrysko, and M. Weidemann, Design and evaluation of shielded gradient coils, *Magn. Reson. Med.* **26,** 191–206 (1992).
15. R. W. Bowtell, G. D. Brown, P. M. Glover, M. McJury, and P. Mansfield, Resolution of cellular structures by NMR microscopy at 11.7 T, *Proc. R. Soc. London A* **333,** 457–467 (1990).
16. R. Bowtell and P. Mansfield, Quiet transverse gradient coils: Lorenz force balanced designs using geometrical similitude, *Magn. Reson. Med.* **34,** 494–497 (1995).
17. M. I. Hrovat and C. G. Wade, NMR pulsed-gradient diffusion measurements. I. Spin-echo stability and gradient calibration, *J. Magn. Reson.* **44,** 62–75 (1981).
18. R. Bowtell and P. Robyr, Abstracts of the International Society of Magnetic Resonance in Medicine, 5th Annual Meeting, Vancouver, p. 55, 1997.
19. J. E. M. Snaar, P. Robyr, and R. Bowtell, Strong gradients for spatially resolved diffusion measurements in low mobility systems, *Magn. Reson. Imaging,* in press.